Structure and electronic structure of S-doped graphitic C_3N_4 investigated by density functional theory*

Chen Gang(陈 刚)[a)b)] and Gao Shang-Peng(高尚鹏)[a)†]

[a)] *Department of Materials Science, Fudan University, Shanghai* 200433, *China*

[b)] *School of Physical Science and Technology, Yunnan University, Kunming* 650091, *China*

(Received 14 June 2012; revised manuscript received 6 July 2012)

The structures of the heptazine-based graphitic C_3N_4 and the S-doped graphitic C_3N_4 are investigated by using the density functional theory with a semi-empirical dispersion correction for the weak long-range interaction between layers. The corrugated structure is found to be energetically favorable for both the pure and the S-doped graphitic C_3N_4. The S doptant is prone to substitute the N atom bonded with only two nearest C atoms. The band structure calculation reveals that this kind of S doping causes a favorable red shift of the light absorption threshold and can improve the electroconductibility and the photocatalytic activity of the graphitic C_3N_4.

Keywords: photocatalyst, C_3N_4, density functional theory, dopant

PACS: 71.20.–b, 71.15.Mb, 71.20.Nr, 61.72.S– **DOI:** 10.1088/1674-1056/21/10/107101

1. Introduction

The photocatalytic reaction utilizes the inexhaustible solar energy to produce hydrogen from water or to clean the environment. Developing new and more efficient photocatalysts is important to address energy shortage and environmental pollution problems. Since Fujishima *et al.* reported that it can decompose water (H_2O) to obtain hydrogen (H_2),[1] titanium dioxide (TiO_2) has attracted extensive attention.[2,3] However, as a wide band gap (3.0 eV–3.2 eV) semiconductor, TiO_2 only shows the photocatalytic activity under the ultraviolent (UV) irradiation. TiO_2 is transparent to visible light, and this restricts its capability to effectively utilize solar energy. Many studies have been devoted to modifying TiO_2 to shift the absorption threshold towards visible light[4−6] or to look for new non-titania-based photocatalysts.[7−10]

As a metal-free photocatalyst, graphitic carbon nitride (g-C_3N_4) can produce H_2 from water under the visible-light irradiation,[10] and it is also reported as a promising candidate in environmental catalysis for NO decomposition.[11] g-C_3N_4 can be prepared by a simple pyrolysis of urea[12] or directly heating melamine,[13] indicating that it is easy and inexpensive to obtain g-C_3N_4. g-C_3N_4 is stable in acid (pH=0) or base (pH=14) conditions due to the strong covalent bond between carbon and nitrogen. These merits of g-C_3N_4 have attracted intense interest.[14−16] However, there are some drawbacks to pure g-C_3N_4 being used as a photocatalyst. Firstly, although the photocatalytic activity under visible light is observed, the band gap of g-C_3N_4 is about 2.7 eV,[10] which means it only absorbs photons with wavelengths shorter than 459 nm (blue light). Secondly, the H_2 evolution of the bare g-C_3N_4 is fluctuant, and the efficiency is low (about 0.1 μmol·h^{-1}–4 μmol·h^{-1}). To improve the photocatalytic activity of g-C_3N_4, some modifications are necessary. It is reported that depositing a small amount of Pt particles could weaken the fluctuant H_2 evolution and improve the H_2 production rate.[10,17] Doping Zn to g-C_3N_4[18] or forming the Ag/g-C_3N_4 hybrid catalyst[19] could also improve the photocatalytic activity and increase the H_2 production rate because metal dopants/particles can capture the photogenerated electrons and create active sites for H_2 production. The non-metal doping of g-C_3N_4 keeps the photocatalytic system metal-free. Boron doped into g-C_3N_4 can decrease the band gap and improve the light absorption ability,[20] phosphorus doped into

*Project supported by the National Basic Research Program of China (Grant No. 2011CB606403) and the Doctoral Fund of the Ministry of Education of China (Grant No. 20090071120062).

†Corresponding author. E-mail: gaosp@fudan.edu.cn

© 2012 Chinese Physical Society and IOP Publishing Ltd

g-C_3N_4 can improve the electrical conductivity.[21] Liu *et al.* reported that sulfur-doped g-C_3N_4 has a unique electronic structure, which can improve the H_2 evolution rate to be 7.2 and 8 times higher than that of pure g-C_3N_4 at light wavelengths longer than 300 nm and 420 nm, respectively.[22]

In order to understand the micromechanism of the photocatalystic process and design better photocatalysts, we need to obtain detailed and accurate information of structure, formation energy, charge density, band structure, density of states, etc. *Ab initio* calculations can be a useful tool in determining the dopant position and the atomic relaxation near the dopant atom and comparing the electronic structures of the pure and the doped g-C_3N_4. In this paper, the structure and the electronic structure of the pure and the S-doped g-C_3N_4 are studied by using the density functional theory (DFT). A semi-empirical correction to the exchange–correlation functional is employed to describe the weak interaction between the g-C_3N_4 layers in determining the equilibrium structure and the formation energy of S dopant in different non-equivalent sites. The difference of electronic structure between undoped and doped g-C_3N_4 is closely examined, and the connection between the electronic structure variation and the photocatalytic property is discussed.

2. Calculation methods

The calculations are based on the CASTEP, a plane-wave pseudopotential code.[23] The correct long-range interaction tail is absent in the popular local-density approximation (LDA) or the generalized gradient approximation (GGA) for the exchange–correlation functionals of DFT, so the standard DFT with LDA or GGA often predicts a considerably larger distance between the graphitic-like layers than the experimental value, or gives a value depending on the initial input and thus gives a random prediction in some cases. In order to describe the weak interaction between the graphitic-like layers of g-C_3N_4 more accurately, we use the DFT with the semi-empirical dispersion–correction scheme (DFT-D).[24,25] The exchange–correlation energy is described by the GGA of PBE type.[26] The plane-wave cutoff energy is chosen to be 310 eV. A 2×2×4 Monkhorst–Pack grid is used for k-point sampling in the first Brillouin zone for the supercell containing 112 atoms. The structural relaxation is conducted using the Broyden–Fletcher–Goldfarb–Shanno (BFGS) method.[27] The symmetry of the structure is lifted off in the geometry optimization to determine the internal positions of atoms and the crystal lattice parameters without any previous assumptions. The convergence tolerances are chosen to be 5.0×10^{-6} eV/atom for energy, 5.0×10^{-4} Å (1 Å=0.1 nm) for maximum displacement, and 0.01 eV/Å for maximum stress. The electronic structure calculation is carried out using the optimized structure.

3. Results and discussion

3.1. Crystal structure

Several potential allotropes of g-C_3N_4 have been proposed according to the repeated unit within each layer and the stacking sequence of layers.[28,29] A heptazine (C_6N_7)-based phase is regarded to be the most stable and usually found g-C_3N_4. We study the heptazine-based phase of g-C_3N_4 in this work. The ideal coplanar heptazine-based g-C_3N_4 belongs to space group *Cmcm*. A supercell including 112 atoms is selected for both the pure and the doped g-C_3N_4. Both the coplanar and the corrugated supercells of g-C_3N_4 are shown in Fig. 1. According to the experimental characterization by Liu *et al.*,[22] the C–S bonds are formed in the framework of C–N bonds by replacing N with S. The doping configurations are shown in Fig. 2. There are three kinds of N atoms (N_{Cen}, N_{Aro}, and N_{Tet} as shown in Fig. 2(a)). The N_{Tet} atom plays an important role in mediating the three nearest heptazine rings. The doped g-C_3N_4 with the S atom substituting the N_{Tet} atom is energetically unfavorable. So we only consider the other two kinds of substitutional sites, i.e., N_{Aro} and N_{Cen} sites. There is one S dopant in the 112-atom supercell.

The optimized structural parameters are shown in Table 1. Note that the lattice constants correspond to the 112-atom supercell. The distance between the adjacent layers in the corrugated g-C_3N_4 is larger than that in the coplanar g-C_3N_4. The energy of the corrugated g-C_3N_4 is lower than that of the coplanar g-C_3N_4, benefiting from avoiding the strong repulsive interactions among lone electron pairs of the N atoms.[30] From the viewpoint of total energy, the corrugated configuration is preferred.

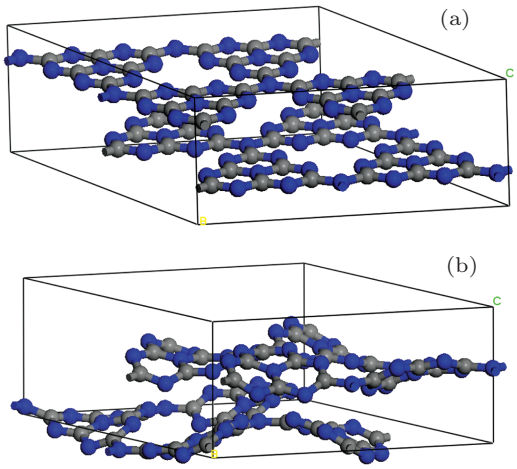


Fig. 1. (colour online) (a) Coplanar and (b) corrugated configurations of the supercell of g-C_3N_4, where C and N atoms are depicted by grey and blue balls, respectively.

The coplanar layer can be maintained when the S atom is doped into the coplanar g-C_3N_4 at the N_{Aro} site (Fig. 2(b)), though a corrugated configuration (Fig. 2(c)) is energetically more stable. The coplanar layers cannot be maintained if the N_{Cen} atom is substituted. So only the corrugated configuration of the S dopant on the N_{Cen} site is considered (Fig. 2(d)). The corrugated g-$C_3N_{3.94}S_{0.06}$ with S sitting at the N_{Aro} site has the lowest energy among the three doping models (Table 1). Just like the corrugated g-C_3N_4, the corrugated g-$C_3N_{3.94}S_{0.06}$ has a larger distance between the adjacent layers than the coplanar g-$C_3N_{3.94}S_{0.06}$(N_{Aro} atom substituted). The analysis of bond length shows that all the C–S bonds in the doped system are longer than the initial C–N bonds in the undoped g-C_3N_4. A bilayer supercell is employed, and the structure changes of the second layer during corrugation are similar to those of the first layer shown in Fig. 2.

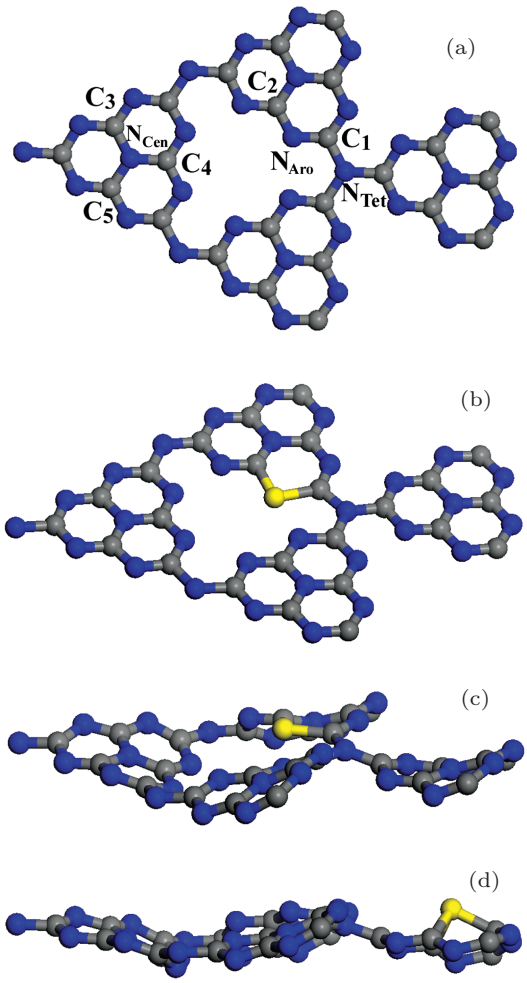


Fig. 2. (colour online) The structure of S-doped g-C_3N_4: (a) schematic view of the doping sites (N_{Aro} and N_{Cen}) and the nearest C atoms, (b) S dopant on the N_{Aro} site with coplanar configuration, (c) S dopant on the N_{Aro} site with corrugated configuration, (d) S dopant on the N_{Cen} site with conrugated configuration. The C, N, and S atoms are depicted by grey, blue, and yellow balls, respectively.

Table 1. Structural parameters and total energies of undoped and doped g-C_3N_4. The total energy of the corrugated g-$C_3N_{3.94}S_{0.06}$ with S dopant on N_{Aro} site is set to 0 eV. The total energy is corresponding to a supercell containing 112 atoms.

	Lattice constant/Å			Angle/(°)			Energy/eV
	a	b	c	α	β	γ	
g-C_3N_4 (coplanar)	14.28	14.28	6.05	90	90	59.98	10.456
g-C_3N_4 (corrugated)	13.83	13.83	6.71	90.46	90.08	60.41	5.303
S dopant on N_{Aro} site (coplanar)	14.36	14.27	6.08	90	90	59.87	4.591
S dopant on N_{Aro} site (corrugated)	13.94	13.83	6.73	91.35	90.55	60.37	0
S dopant on N_{Cen} site	13.86	13.86	6.73	90.70	91.08	60.28	0.530

The impurity formation energy can be calculated as

$$E_f = E[C_{48}N_{63}S] - E[C_{48}N_{64}] - \mu_S + \mu_N, \quad (1)$$

where $E[C_{48}N_{63}S]$ and $E[C_{48}N_{64}]$ are the total energies of the doped and the undoped systems, respectively, μ_N and μ_S are the chemical potentials of N and S, respectively. As an approximation, we simply

take the chemical potentials of N in N_2 and S in bulk sulfur for μ_N in g-C_3N_4 and μ_S in dopant source. As the corrugated configuration is energetically favorable, the formation energy for S substituting the N_{Aro} atom (1.17 eV) is smaller than that for S substituting the N_{Cen} atom (1.70 eV). So it is more favorable for S to substitute the N_{Aro} atom than the N_{Cen} atom. The positive impurity formation energy shows that both kinds of substitutions are difficult. Our calculated formation energies qualitatively agree with those reported by Liu *et al.*[22]

3.2. Electronic structure

Atomic charges obtained by the Mulliken analysis for dopant atoms on different sites and its nearest neighbors are given in Table 2. Because the electronegativity of N is lower than that of C, the N atoms in pure g-C_3N_4 attract more valence electrons as compared to the C atoms, so the C atomic charge is positive, and the N atomic charge is negative. Note that the atomic charge of the C_4 atom is different from that of C_2, C_3, and C_5 atoms, although they are all bonding with two N_{Aro} and one N_{Cen} atoms. The C_4 atom is different from the others when the nearest layers are taken into account. The C_4 atom is sitting nearly on the top of a C atom in the nearest layer, whereas C_2, C_3, and C_5 are sitting on the top of voids between the heptazine rings. So the chemical environment of the C_4 atom is different from that of C_2, C_3, and C_5 atoms, and this results in the different atomic charges.

Table 2. Atomic charges obtained by the Mulliken analysis for C atoms near the dopant site and for S dopant and N atom before and after the substitution.

	N_{Tet}	C_1	C_2	N_{Aro}	S_{Aro}	C_3	C_4	C_5	N_{Cen}	S_{Cen}
g-C_3N_4 (coplanar)	–0.28	0.45	0.52	–0.38		0.52	0.48	0.52	-0.29	
g-C_3N_4 (corrugated)	–0.28	0.48	0.52	–0.40		0.52	0.51	0.52	-0.30	
S dopant on N_{Aro} site (coplanar)	–0.26	0.13	0.20		0.49	0.52	0.48	0.52	-0.29	
S dopant on N_{Aro} site (corrugated)	–0.26	0.15	0.19		0.47	0.51	0.51	0.52	-0.30	
S dopant on N_{Cen} site	–0.27	0.48	0.51	–0.42		0.25	0.24	0.21		0.54

After the N atom is substituted by the S atom, there is no distinct valence electron transfer between the S dopant and its nearest C atoms due to the similar electronegativities of S (Pauling's electronegativity 2.58) and C (Pauling's electronegativity 2.55) atoms. The atomic population values of all the S dopants and its nearest C atoms are positive, indicating that all of them lose valence electrons after S is doped (Table 2). The population of the C–S bond is smaller than that of the original C–N bond (Table 3). It indicates that the C–S bond is obviously weaker than the C–N bond. The S dopant has more valence electrons but forms weaker covalent bonds with the nearest C atoms.

Table 3. Bond populations obtained by the Mulliken analysis in pure and doped g-C_3N_4.

	C_1–N_{Aro} (C_1–S_{Aro})	C_2–N_{Aro} (C_2–S_{Aro})	C_3–N_{Cen} (C_3–S_{Cen})	C_4–N_{Cen} (C_4–S_{Cen})	C_5–N_{Cen} (C_5–S_{Cen})
g-C_3N_4 (coplanar)	1.03	1.08	0.83	0.83	0.83
g-C_3N_4 (corrugated)	1.04	1.05	0.83	0.84	0.85
S dopant on N_{Aro} site (coplanar)	0.44	0.69			
S dopant on N_{Aro} site (corrugated)	0.61	0.67			
S dopant on N_{Cen} site			0.48	0.49	0.58

In order to investigate the influences of the S dopant on different sites, the band structures of pure- and S-doped g-C_3N_4 are shown in Figs. 3–5. Although the coplanar structures are less stable from the viewpoint of total energy, their band structures are also shown in Figs. 3 and 4, because the coplanar structure has been discussed in many literatures and a comparison between the band structures of coplanar and corrugated structures is helpful for understanding the effect of corrugation.

The lowest conduction band (band A) and the highest valence band (band B) are depicted by lines with open squares. Our calculations are based on the DFT-GGA predict direct band gaps of 1.10 eV (Fig. 3(a)) and 1.55 eV (Fig. 3(b)) for coplanar and corrugated g-C_3N_4, respectively. The theoretical band gap is smaller than the experimental reported value of 2.7 eV[10] and the theoretical band gap of 2.88 eV from the GW method.[31] It is a well-known problem that the DFT–LDA or DFT–GGA will underestimate the band gap. But this will not hinder us to analyze the relative change of the band structure induced by the S dopant on different sites.

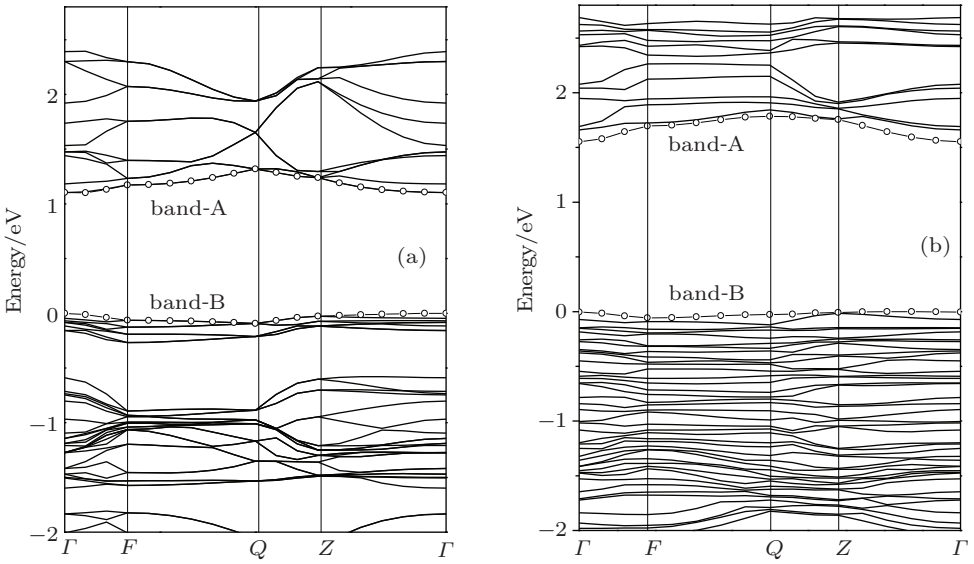


Fig. 3. Band structures of (a) coplanar and (b) corrugated g-C_3N_4.

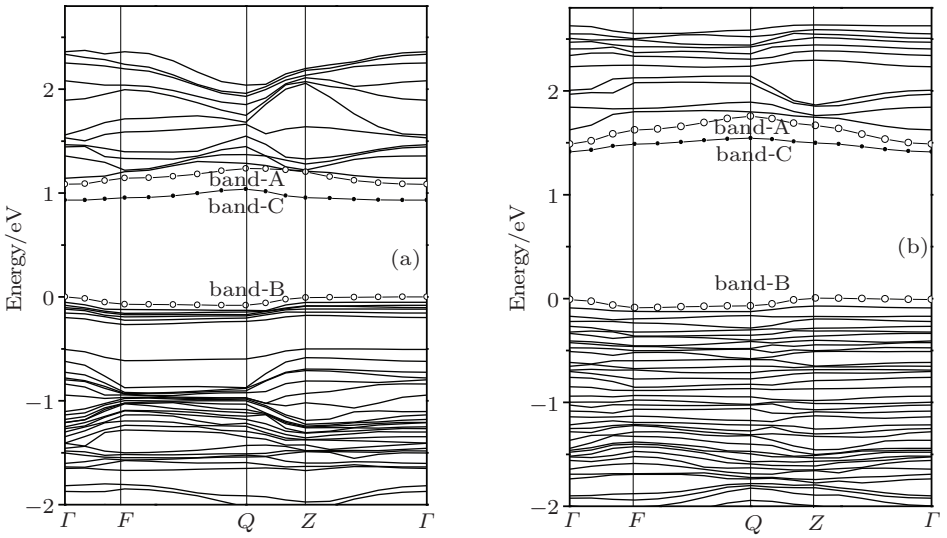


Fig. 4. Band structures of S-doped g-C_3N_4 with S dopant substituted the N_{Aro} atom in (a) coplanar (b) corrugated configurations.

Figure 4 shows the band structures of coplanar and corrugated g-C_3N_4 with the N_{Aro} atom substituted by the S atom. A new band (band C) appears between bands A and B. The partially-filled band C can be found at the upper range of the band gap and is close to band A of the S-doped g-C_3N_4, implying an n-type doping. A density of states analysis (Figs. 6(c) and 6(d)) shows that band C is mainly composed of the p orbital of the S atom. The energy difference between bands C and A is smaller than the band gap

of the undoped g-C_3N_4. Keeping in mind that the DFT–GGA underestimates the band gap and the experimental reported band gap is 2.7 eV for g-C_3N_4, we know that this red shift of optical excitation threshold coming from the S substitution of the N_{Aro} atom will enable the g-C_3N_4 photocatalyst to make better use of the visible light. It is one of the key purposes of modifying the photocatalyst with a wide band gap. The partially-filled band C just below band A can provide more electrons for band A via thermal excitation. This is favorable for increasing the probability of capturing electrons for H^+. So the doped g-C_3N_4 with S substituted the N_{Aro} atom can achieve a higher hydrogen generation efficiency than the pure g-C_3N_4.

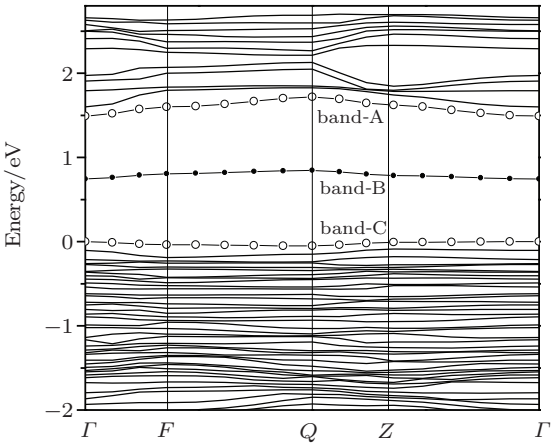


Fig. 5. Band structure of S-doped g-C_3N_4 with S dopant substituted the N_{Cen} atom.

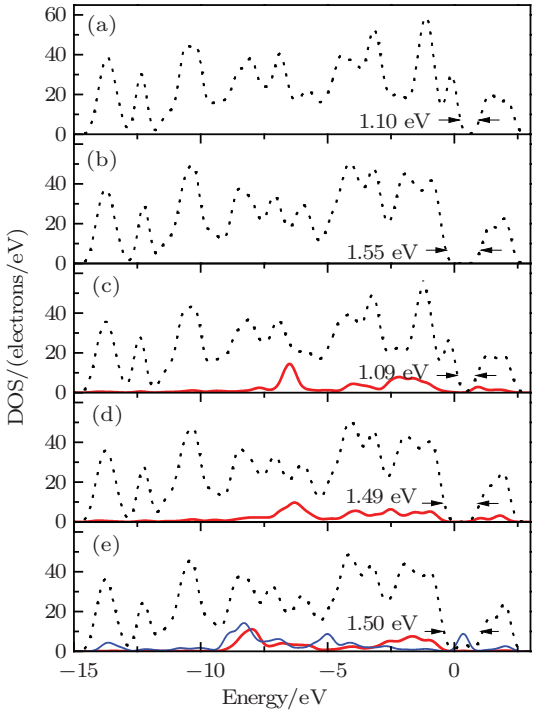


Fig. 6. (colour online) Density of states (DOS) analysis for g-C_3N_4: (a) total DOS of coplanar g-C_3N_4, (b) total DOS of corrugated g-C_3N_4, (c) total DOS and S partial DOS of coplanar g-C_3N_4 with S dopant occupied the N_{Aro} site, (d) total DOS (dotted line) and S partial DOS (red thick line) of corrugated g-C_3N_4 with S dopant occupied the N_{Aro} site, (e) total DOS (dotted line), S partial DOS (red thick line), and C (near S dopant) partial DOS (blue thin line) of g-C_3N_4 with S dopant occupied the N_{Cen} site. The S partial DOS is enlarged 10 times and the C partial DOS is enlarged 20 times for easy visualization.

When the S dopant substitutes the N_{Cen} atom sitting at the center of the three nearest C atoms, only the corrugated configuration is possible. In the band structure (Fig. 5), a new band C lies at the middle of the band gap. The partial density of states (PDOS) analysis (Fig. 6(e)) shows that the partially-filled band C mainly corresponds to the p orbitals of the C atoms near the S dopant. Though band C can also reduce the threshold energy to absorb light and thus can make use of visible light photon with smaller energy, this kind of deep level also captures the photon excited carriers and acts as an effective recombination center of electron–hole pair. So this type of doping is unfavorable for the photocatalyzed H_2 generation.

4. Conclusion

The structure and the electronic structure of pure and S-doped g-C_3N_4 have been investigated. The corrugated configuration of the heptazine-based g-C_3N_4 is energetically favorable compared to the coplanar configuration. When a S atom substitutes the N_{Aro} atom bonded only with two nearest C atoms in g-C_3N_4, the electronic structure analysis shows that the impurity energy level lies just below the CBM. So the S dopant on the N_{Aro} site can provide electrons to the conduction band and cause a favorable red shift of the light absorption threshold. This can improve the electroconductibility and the photocatalytic activity. If the N_{Cen} atom, which is bonded with its three nearest C atoms, is substituted by S, a deep energy level is found to lie at the middle of the band gap. This deep level can act as a recombination center of electron–hole pairs and deteriorates the photocatalytic activity. The impurity formation energy analysis shows that it is easier for S substituting the N_{Aro} atom than substituting the N_{Cen} atom. So when S is doped into g-C_3N_4, S dopant favorably occupies the N_{Aro} atom site, and this is the doping mechanism that can improve the photocatalytic activity.

References

[1] Fujishima A and Honda K 1972 *Nature* **238** 37

[2] Ni M, Leung M K H, Leung D Y C and Sumathy K 2007 *Renew. Sust. Energ.* **11** 401

[3] Gnaser H, Huber B and Ziegler C 2004 "Nanocrystalline TiO2 for Photocatalysis", in: Nalwa H S ed. *Encyclopedia of Nanoscience and Nanotechnology* Vol. 6, pp. 505–535

[4] Asahi R, Morikawa T, Ohwaki T, Aoki K and Taga Y 2001 *Science* **293** 269

[5] Lin Y M, Jiang Z Y, Hu X Y, Zhang X D, Fan J, Miao H and Shang Y B 2012 *Chin. Phys.* B **21** 033103

[6] Gao P, Wu J, Liu Q J and Zhou W F 2010 *Chin. Phys.* B **19** 087103

[7] Yi Z, Ye J, Kikugawa N, Kako T, Ouyang S, Stuart-Williams H, Yang H, Cao J, Luo W, Li Z, Liu Y and Withers R L 2010 *Nat. Mater.* **9** 559

[8] Kale B B, Baeg J O, Lee S M, Chang H, Moon S J and Lee C W 2006 *Adv. Funct. Mater.* **16** 1349

[9] Zhang L, Djerdj I, Cao M, Antonietti M and Niederberger M 2007 *Adv. Mater.* **19** 2083

[10] Wang X, Maeda K, Thomas A, Takanabe K, Xin G, Carlsson J M, Domen K and Antonietti M 2009 *Nat. Mater.* **8** 76

[11] Zhu J, Wei Y, Chen W, Zhao Z and Thomas A 2010 *Chem. Commun.* **46** 6965

[12] Liu J, Zhang T, Wang Z, Dawson G and Chen W 2011 *J. Mater. Chem.* **21** 14398

[13] Yan S C, Li Z S and Zou Z G 2009 *Langmuir* **25** 10397

[14] Ge L 2011 *Mater. Lett.* **65** 2652

[15] Zhang J, Chen X, Takanabe K, Maeda K, Domen K, Epping J D, Fu X, Antonietti M and Wang X 2010 *Angew. Chem. Int. Ed.* **49** 441

[16] Sehnert J, Baerwinkel K and Senker J 2007 *J. Phys. Chem.* B **111** 10671

[17] Maeda K, Wang X, Nishihara Y, Lu D, Antonietti M and Domen K 2009 *J. Phys. Chem.* C **113** 4940

[18] Yue B, Li Q, Iwai H, Kako T and Ye J 2011 *Sci. Technol. Adv. Mater.* **12** 034401

[19] Ge L, Han C, Liu J and Li Y 2011 *Appl. Catal.* A: *Gen.* **409–410** 215

[20] Yan S C, Li Z S and Zou Z G 2010 *Langmuir* **26** 3894

[21] Zhang Y, Mori T, Ye J and Antonietti M 2010 *J. Am. Chem. Soc.* **132** 6294

[22] Liu G, Niu P, Sun C, Smith S C, Chen Z, Lu G Q and Cheng H M 2010 *J. Am. Chem. Soc.* **132** 11642

[23] Clark S J, Segall M D, Pickard C J, Hasnip P J, Probert M J, Refson K and Payne M C 2005 *Z. Kristallogr.* **220** 567

[24] Tkatchenko A and Scheffler M 2009 *Phys. Rev. Lett.* **102** 073005

[25] Grimme S, Antony J, Ehrlich S and Krieg H 2010 *J. Chem. Phys.* **132** 154104.

[26] Perdew J P, Burke K and Ernzerhof M 1996 *Phys. Rev. Lett.* **77** 3865

[27] Pfrommer B G, Côté M, Louie S G and Cohen M L 1997 *J. Comput. Phys.* **131** 233

[28] Kroke E and Schwarz M 2004 *Coordin. Chem. Rev.* **248** 493

[29] Thomas A, Fischer A, Goettmann F, Antonietti M, Müller J O, Schlögl R and Carlsson J M 2008 *J. Mater. Chem.* **18** 4893

[30] Gracia J and Kroll P 2009 *J. Mater. Chem.* **19** 3013

[31] Xu Y and Gao S P 2012 *Int. J. Hydrogen Energy* **37** 11072